PCCP

ROYAL SOCIETY OF CHEMISTRY

PAPER

View Article Online
View Journal | View Issue

Cite this: *Phys. Chem. Chem. Phys.*, 2025, **27**, 25422

Oxidation-induced σ-aromaticity in halogenated cycloalkanes

Slavko Radenković * and Slađana Đorđević

Received 14th August 2025,
Accepted 1st November 2025

DOI: 10.1039/d5cp03126e

rsc.li/pccp

In this study, we investigated a series of dicationic halogenated cycloalkanes with the general formula $C_nH_nX_n^{2+}$ (n = 4, 5, 6, and 7, and X = Br and I), where halogen substituents are positioned on each carbon atom, forming a cyclic structure. To assess potential σ-aromaticity within the halogen atom rings, we employed magnetically induced current density (MICD) calculations, the electron density of delocalized bonds (EDDB) and aromatic stabilization energy (ASE), as an energetic descriptor. Our results revealed significant σ-electron delocalization throughout the halogen atom rings, consistently supported by all applied aromaticity indices. This way, we showed that nonaromatic, neutral halogenated cycloalkanes can be converted into σ-aromatic dicationic species through conventional oxidation procedures. Furthermore, we demonstrated that this σ-electron delocalization closely resembles that observed in the prototypical double aromatic system $C_6I_6^{2+}$. Interestingly, the observed σ-aromaticity found in the studied dications does not always conform to Hückel's rule. These results can be rationalized in the context of selection rules governing virtual transitions between occupied and unoccupied molecular orbitals.

Introduction

The concept of aromaticity traces its roots to the discovery of benzene by Michael Faraday two centuries ago. Since then, the idea has undergone significant development, evolving into a fundamental concept in chemistry. Aromaticity profoundly enhanced our understanding of molecular electronic structures and reactivity in both ground[1–4] and excited states.[5,6] Traditionally, aromaticity was associated with organic, conjugated (poly)cyclic compounds. A key extension of the concept was recognition that σ-electrons, like π-electrons, can also participate in cyclic delocalization, leading to the notion of σ-aromaticity.[7–11] In 1979, Schleyer introduced the idea of double aromaticity, proposing that the cationic species $C_6H_3^+$ could exhibit both π- and σ-aromaticity simultaneously.[12] This hypothesis was later confirmed by the successful synthesis of $C_6H_3^+$ by Nelson and Kenttämaa.[13] The concept of double aromaticity was further corroborated by Sagl and Martin through their synthesis and characterization of the dication $C_6I_6^{2+}$.[14] Their seminal work demonstrated that the cationic $C_6I_6^{2+}$ is a stable system with a singlet ground state, displaying both π- and σ-aromaticity according to the geometric and magnetic properties. The double aromaticity of $C_6I_6^{2+}$ was a subject of extensive computational studies.[15–17] More recently, Saito *et al.*[18] experimentally characterized the hexakis(phenylselenyl)benzene dication, a molecule composed of a π-aromatic benzene core surrounded by a σ-aromatic selenium ring. Double aromaticity can occur in a range of molecular structures, some of which do not necessarily contain a benzene ring.[19–21] These discoveries revealed the significance of double aromaticity as a powerful tool for rationalizing the structure and stability of a wide variety of systems,[22,23] including boron clusters[24–26] and monocyclic carbon clusters.[27–30]

In our recent study,[31] we demonstrated that the carbon atom ring size is the primary factor governing the appearance of oxidation-induced σ-aromaticity in periodo-derivatives of monocyclic conjugated hydrocarbons, resulting in double aromatic character. This structural parameter determines the distance between iodine atoms, and, consequently, the extent of overlap between their in-plane lone pair orbitals. Furthermore, we found that the oxidation of the periodo-derivatives of polycyclic conjugated hydrocarbons can induce σ-aromaticity in the iodine-based macrocyclic rings, even in the presence of significant nonplanarity in the carbon-based core polycyclic unit. Notably, σ-aromaticity has primarily been observed in all-metal systems. Motivated by our recent study,[31] the present work explores the possibility of σ-aromaticity in oxidized halogenated cycloalkanes, where halogen atoms are arranged to form a cyclic structure. Specifically, we investigated a series of dicationic halogenated cycloalkanes with the general formula $C_nH_nX_n^{2+}$ (n = 4, 5, 6, and 7, and X = Br and I), as illustrated in Fig. 1. Our research addresses the following central questions: (a) can oxidation of nonaromatic halogenated cycloalkanes induce σ-aromaticity analogous to that observed in the prototypical double aromatic system $C_6I_6^{2+}$? (b) Is the aromatic

University of Kragujevac, Faculty of Science, P. O. Box 60, 34000 Kragujevac, Serbia. E-mail: slavkoradenkovic@kg.ac.rs

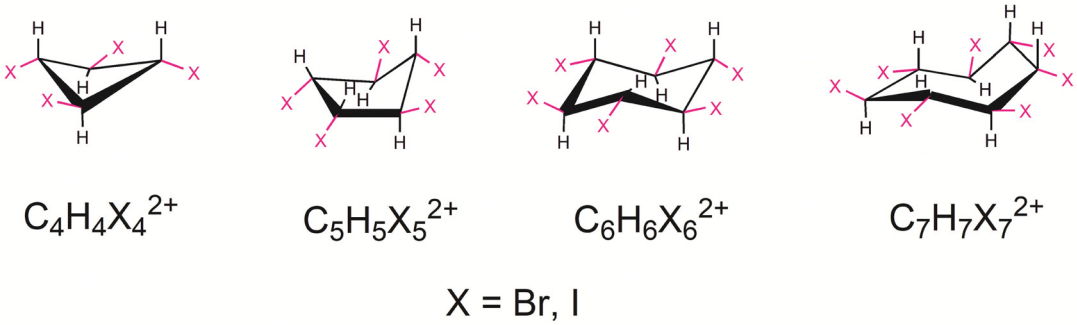

Fig. 1 Structures of the dicationic halogenated cycloalkanes investigated in this study.

character of the central mono- or polycyclic carbon framework a necessary condition for inducing σ-electron aromaticity in halogen atom rings? It is worth noting that some of the cycloalkanes, such as cyclopropane and cyclobutane, have been proposed to exhibit σ-electron aromaticity and antiaromaticity, respectively.[7,8] However, while this topic has been much studied, no compelling energetic evidence has been found to support significant σ-electron aromaticity or antiaromaticity in these systems.[32] Moreover, their magnetic properties appear to be largely unaffected by σ-electron ring currents.[33] Our selected systems offer a valuable platform to assess how the ring size and geometry affect the σ-aromaticity of doubly oxidized species. We focus on bromine and iodine derivatives based on previous findings that double aromaticity has been observed only in perbromo- and periodo-benzene derivatives, while analogous perfluoro- and perchloro-dications do not exhibit notable σ-electron delocalization.[15,17] Previous studies have also suggested that Hückel's rule,[34] traditionally applied to π-conjugated systems, can be extended to certain σ-aromatic systems.[9] However, as will be shown below, the σ-aromaticity observed in the investigated dications (Fig. 1) does not always conform to Hückel's rule. In this work, aromaticity was primarily assessed through the analysis of magnetically induced current densities (MICDs),[35,36] supported by the electron density of delocalized bonds (EDDB)[37,38] as an electronic aromaticity index and by aromatic stabilization energy (ASE)[2,39] as an energetic descriptor. Finally, we demonstrate that the obtained results can be rationalized through the analysis of virtual transitions between occupied and unoccupied molecular orbitals.[40,41] This approach offers insight into the relationship between the molecular electronic structure and magnetic aromaticity and can explain why Hückel's rule may not universally apply to σ-aromatic systems.

Computational methods

Geometry optimizations and vibrational frequency calculations for all studied molecules were carried out using the B3LYP/def2-TZVP[42–45] level of theory, as implemented in the Gaussian 09 program package.[46] The magnetically induced current density (MICD) was computed at the same level of theory using the diamagnetic zero (DZ) version of the continuous transformation of the origin of current density (CTOCD) method.[40,47–49] In the resulting MICD maps, clockwise and counterclockwise current circulations correspond to diatropic and paratropic currents, respectively. These maps were generated using ParaView software.[50] Current strengths (I, in nA T^{-1})[51] were determined by numerical integration of the current density through a rectangle bisecting the bond of interest perpendicularly. Diatropic and paratropic currents contribute positively and negatively to the current strength, respectively. MICD calculations were performed using an in-house FORTRAN program, which utilizes Gaussian-wfx files as the input. The def2-TZVP basis set includes the Stuttgart fully relativistic effective core potentials (ECPs)[52] for iodine atoms to account for relativistic effects. Although relativistic effects have shown to be noticeable in the MICD calculations for C_6Br_6 and C_6I_6, they are not essential for obtaining qualitatively correct results.[53] Furthermore, it has been demonstrated that the choice of functional and the size of the basis set have only a minor influence on MICD results in per-halogenated aromatic compounds.[17,31]

The electron density of delocalized bonds (EDDB)[37,38] was calculated using the charge and bond order matrix obtained from natural bond orbital (NBO) analysis,[54] performed at the B3LYP/def2-TZVP level of theory using Gaussian 09. $EDDB_H$ values were calculated using the RunEDDB code.[55]

The aromatic stabilization energies[2,39] were estimated through a series of properly constructed homodesmotic reactions.

Planarity deviations of the studied molecules were assessed using the brute-force planarity index (BFPI),[56] defined as the average distance of all (or a specified subset of) atoms from the best-fit plane obtained by minimizing that distance in the given molecule.

Results and discussion

The top and side views of the optimized geometries of the dications $C_nH_nX_n^{2+}$ (n = 4, 5, 6, and 7, and X = Br and I) are shown in Fig. S1 and S2. A detailed analysis of these geometries reveals that both Br- and I-substituted derivatives exhibit very similar structural features. The primary factor influencing the geometry is the size of the central carbon rings, rather than the identity of the halogen atom. Fig. 2 presents the key geometric parameters of the iodinated species, while the corresponding

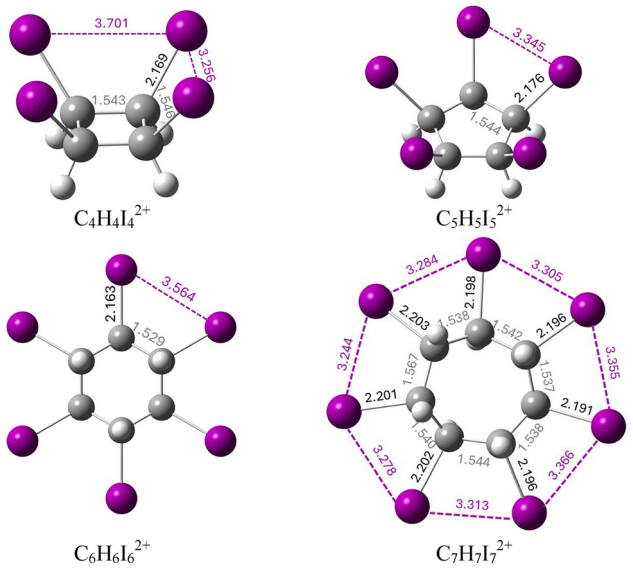

Fig. 2 Optimized geometries of dicationic iodo-cycloalkanes, showing key interatomic distances (in Å).

data for the brominated analogues are provided in Fig. S3. In $C_5H_5I_5^{2+}$ and $C_6H_6I_6^{2+}$, all I–I distances are equivalent, being 3.345 Å and 3.564 Å, respectively, while $C_7H_7I_7^{2+}$ exhibits a slight variation in I–I distances, ranging from 3.278 Å to 3.366 Å. Despite these variations, all observed I–I distances are remarkably close to the reference value of 3.475 Å, obtained at the same level of theory for the prototypical double aromatic species $C_6I_6^{2+}$.[31] Notably, in $C_4H_4I_4^{2+}$, the four-membered iodine ring displays reduced symmetry, with two distinct I–I distances: a longer one of 3.701 Å and a shorter one of 3.256 Å. An analogous pattern is observed in the Br-substituted dications (Fig. S3), where Br–Br distances are slightly shorter than the corresponding I–I distances. Furthermore, the C–C bond lengths are highly consistent among molecules with the same ring size and appear largely unaffected by the nature of the halogen substituents.

Another notable geometric feature of the studied dications, evident from the optimized structures shown in Fig. S1 and S2, is the strong tendency of both bromine and iodine atom rings to adopt planar conformations. To quantify deviations from planarity, the brute-force planarity index (BFPI)[56] was employed (Table 1). The BFPI values indicate that the four- and five-membered Br- and I-containing rings are essentially planar, while the largest deviation from planarity occurs in the six-membered Br and I rings. Importantly, the four- and five-membered carbon-atom rings in the dications are found to be nearly planar, in contrast to their neutral counterparts. For comparison, we also optimized the structures of the corresponding neutral halogenated cycloalkanes, from which the dications can be formally derived by removing two electrons (Fig. S4 and S5). It is worth noting that some of these neutral structures do not represent the most stable conformers. The neutral structures were intentionally constructed to closely mimic the spatial arrangement of halogen atoms found in the corresponding dications. Fig. S6 compares the geometries

Table 1 Calculated BFPI values (in Å) for the carbon and halogen atom rings of the studied halogenated cycloalkanes in their neutral and dicationic forms

	C-ring		X-ring (X = I, Br)	
	Neutral	Dicationic	Neutral	Dicationic
$C_4H_4Br_4$	1.198	0.001	5.332	0.008
$C_5H_5Br_5$	1.294	0.006	4.500	0.025
$C_6H_6Br_6$	1.973	2.531	6.687	2.369
$C_7H_7Br_7$	2.979	2.452	11.093	1.529
$C_4H_4I_4$	1.198	0.000	4.737	0.001
$C_5H_5I_5$	1.295	0.002	4.025	0.009
$C_6H_6I_6$	2.051	2.545	5.514	2.313
$C_7H_7I_7$	2.595	2.490	7.655	0.820

and relative energies of the conformers presented in Fig. S4 and S5, along with more stable conformers of the four- and five-membered ring systems. Key bond distances and BFPI values for the neutral species are presented in Fig. S7 and Table 1. Upon oxidation, a significant shortening of both I–I and Br–Br distances is observed. Generally, the carbon–carbon bonds also contract, although to a noticeably lesser extent. Moreover, oxidation substantially increases the planarity of both halogen and carbon rings. The only exceptions are the six-membered carbon rings, which retain similar geometries in both the neutral and oxidized forms, as reflected by their comparable BFPI values.

Fig. 3 and Fig. S8 show the overlap integral values between the pre-orthogonal natural bond orbitals (PNBOs)[54] corresponding to the in-plane lone-pairs on I- and Br-atoms. For each halogen atom, both in the neutral and doubly oxidized species, it is straightforward to identify PNBOs representing the in-plane lone pair orbitals. Due to the central symmetry of the molecules studied, these in-plane lone pairs on the iodine and bromine atoms can be described as tangential p-atomic orbitals. The PNBOs for $C_6H_6I_6$ and $C_6H_6I_6^{2+}$ are illustrated in Fig. S9. The planar or nearly planar conformations of the halogen atom rings, combined with relatively short halogen–halogen distances, facilitate significant overlap between the in-plane lone pairs on halogen atoms in the dicationic form. The values given in parentheses in Fig. 3 correspond to the overlap integral values between the in-plane PNBOs in the neutral molecules. These values confirm that oxidation induces such structural changes that enhance the overlap between in-plane lone-pair orbitals, which primarily correspond to the 4p and 5p atomic orbitals on bromine and iodine, respectively.

Fig. 4 displays the canonical molecular orbitals (MOs) describing the σ-electron delocalization along the iodine ring in $C_6H_6I_6^{2+}$. As demonstrated in our previous study,[31] when the overlap between iodine 5p atomic orbitals is sufficiently strong, the highest-energy σ-type MO can become the highest occupied molecular orbital (HOMO) in the neutral precursor. Upon oxidation, two electrons are removed from this orbital, and it becomes the lowest unoccupied molecular orbital (LUMO) in the resulting dication. Fig. 3 and Fig. S8 further illustrate that the overlap between the in-plane lone-pair orbitals on halogen atoms is indeed large enough to produce such σ-type LUMOs in

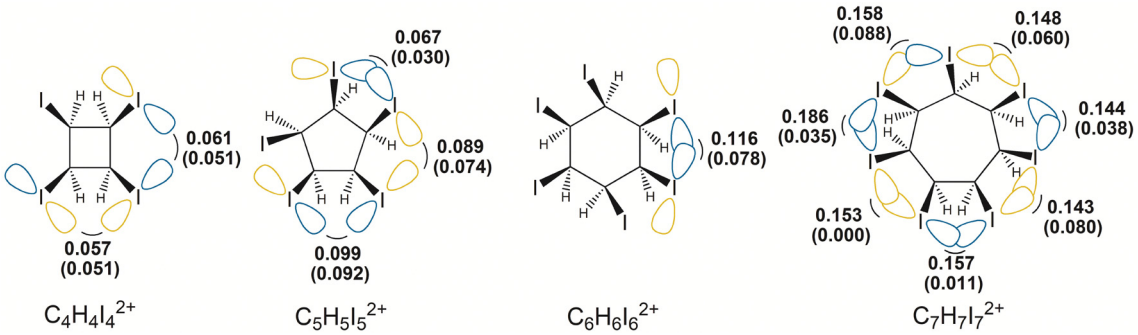

Fig. 3 Absolute values of the overlap integrals between in-plane lone pair PNBOs on iodine atoms in dicationic iodo-cycloalkanes. Values in parentheses correspond to the neutral species.

all examined dications. These LUMOs consistently exhibit strong antibonding character. As shown in Fig. 4, there are ten σ-electrons delocalized along the iodine ring in $C_6H_6I_6^{2+}$, as well as in $C_6H_6Br_6^{2+}$ (Fig. S10). Similarly, $C_5H_5I_5^{2+}$ and $C_5H_5Br_5^{2+}$ each possess eight delocalized σ-electrons (Fig. S10). Based on the analysis of the σ-delocalized canonical MOs in these systems, we found that, for each dication $C_nH_nX_n^{2+}$ (n = 4, 5, 6, and 7, and X = Br and I), the number of cyclically delocalized σ-electrons follows the general formula $2n - 2$. For all examined dicationic species, the σ-LUMOs have clear analogues among the occupied σ-MOs of the corresponding neutral molecules (Fig. S11).

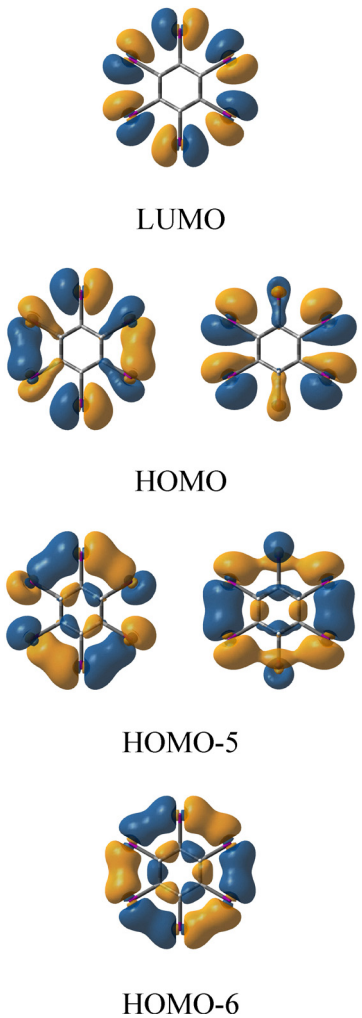

Fig. 4 Canonical σ-type molecular orbitals of $C_6H_6I_6^{2+}$ obtained at the B3LYP/def2-TZVP level of theory.

Visualizing the signed modulus of the calculated magnetically induced current densities is particularly valuable for nonplanar systems, especially those exhibiting central symmetry.[57] In these plots, diatropic currents are shown in blue and paratropic currents in red. As an illustration, Fig. 5 presents the signed modulus of the current density for the neutral and doubly oxidized species $C_6H_6I_6$ and $C_7H_7Br_7$. These plots reveal a clear distinction in the current density distribution between the neutral and oxidized forms. In both dications, $C_6H_6I_6^{2+}$ and $C_7H_7Br_7^{2+}$, strong global diatropic currents are observed along the perimeter formed by the halogen atoms. In contrast, the corresponding neutral species exhibit only localized circulations around individual halogen atoms. Similar global current density circulations are found in the five-, six- and seven-membered rings formed by iodine and bromine atoms in the dicationic species (Fig. S12). An exception is observed in the case of the four-membered rings of $C_4H_4I_4^{2+}$ and $C_4H_4Br_4^{2+}$, where the current density is not uniformly distributed, but instead tends toward a slightly localized pattern (Fig. S12). A more detailed depiction of the current density distribution can be obtained by plotting the current density vectors on the surface, which adopt the shape of molecules (Fig. 6 and 7). Due to the pronounced nonplanarity of the neutral molecules, these maps are sometimes less clear. As shown in Fig. S13, the absence of global circulations and the presence of the localized halogen-centered currents in $C_6H_6I_6$ clearly illustrate this behavior. Notably, the vector plots further confirm that, with the exception of the four-membered ring systems, the dicationic species display pronounced diatropic circulations around halogen atom rings.

To obtain more quantitative insight into the induced current densities, an analysis based on integrated current strengths was performed. For polycyclic systems, such as the molecules studied here, bond current strength profiles offer particularly valuable information.[17] The bond current strength profiles for both the neutral and doubly oxidized forms of the investigated

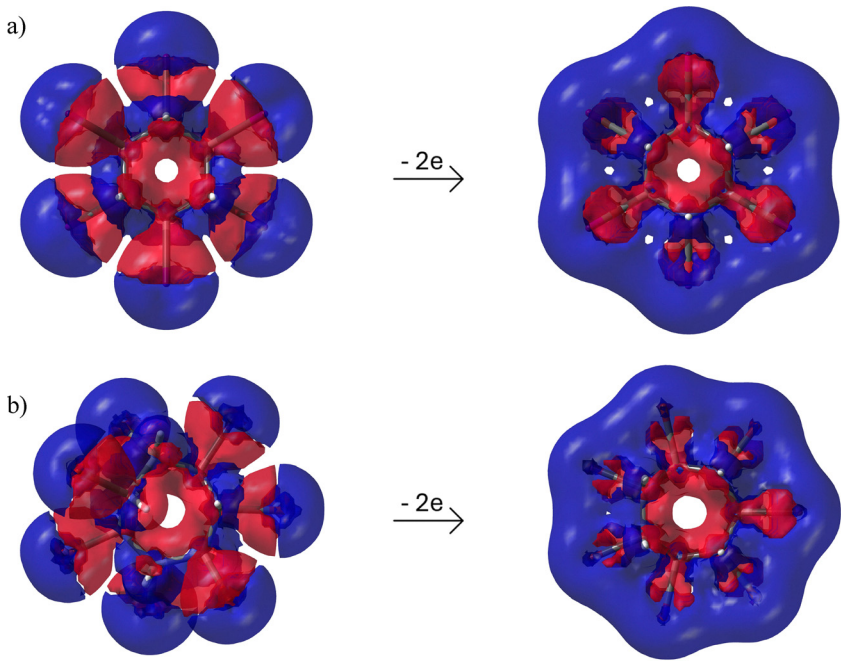

Fig. 5 Signed modulus of the magnetically induced current density in the neutral and dicationic (oxidized) forms of $C_6H_6I_6$ (a) and $C_7H_7Br_7$ (b). The diatropic current density is shown in blue and the paratropic one in red. The isosurface value is set to ±0.02 a.u.

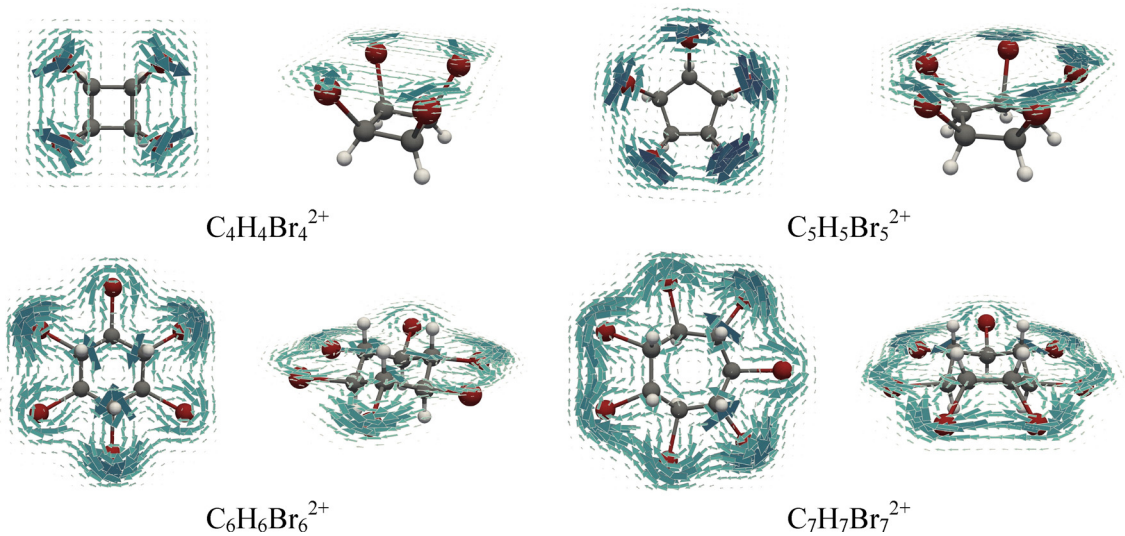

Fig. 6 Top and side views of the total current density maps plotted 1 Bohr above the surface, which adopts the bromine-atom ring shape in the dicationic bromo-substituted cycloalkanes.

molecules are presented in Fig. S14 and S15. The bond current strength profiles of the bromine and iodine derivatives reveal the presence of paratropic currents inside the cycloalkane rings and diatropic currents outside them. These opposing circulations exhibit comparable intensities in both the neutral (blue line in Fig. S14 and S15) and dicationic (purple line in Fig. S14 and S15) forms. Such current density distribution is a characteristic signature of σ-electron contributions to the current strength of C–C bonds. This σ-contribution vanishes at a distance of approximately 2 Å from the ring center. Beyond this distance ($r > 2$ Å), the current strength profiles indicate a significant difference between the neutral and oxidized species. While the neutral forms show negligible current density in this region (for $r > 2$ Å), the dicationic species exhibit strong current densities originating from the σ-MOs associated with the bromine- and iodine-atom rings. These profiles demonstrate that oxidation of halogenated cycloalkanes induces a significant change in the magnetic response of the σ-electron system along the halogen atom rings, while the σ-electron response along the carbon-atom rings remains largely unchanged.

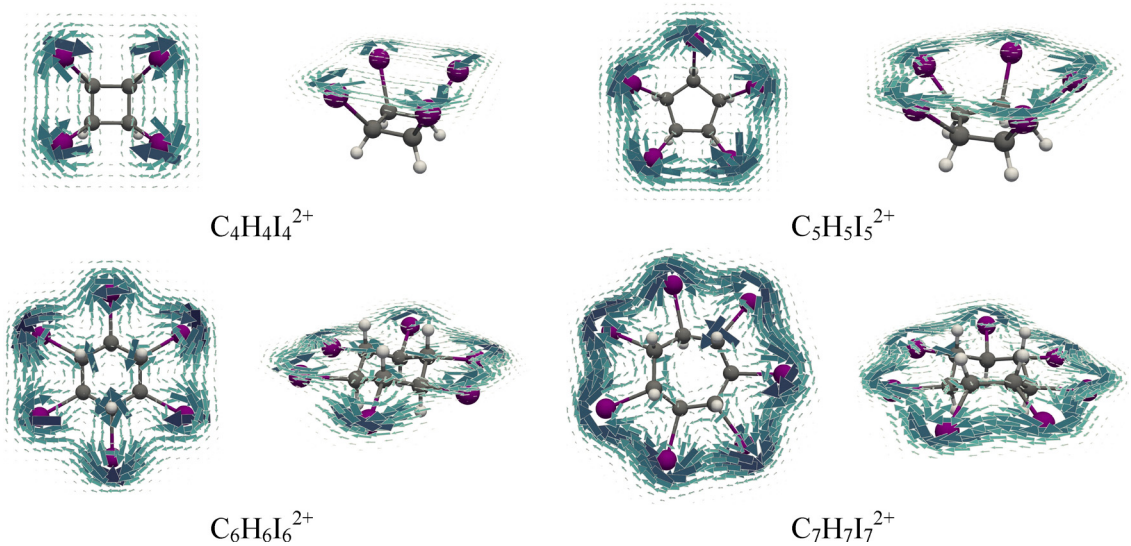

Fig. 7 Top and side views of the total current density maps plotted 1 Bohr above the surface, which adopts the iodine-atom ring shape in the dicationic iodo-substituted cycloalkanes.

The shape of the profile curves was used to define an integration surface that separates the total currents into two distinct contributions: one circulating around the carbon-atom ring and the other around the halogen-atom ring. To achieve this, the integration surface was divided into two regions (Fig. S14 and S15). The first region, corresponding to the circulations around the carbon-atom ring, extends from the ring center (r = 0 Å) to the position of the second minimum in the profile curves ($r \approx 2$ Å). The second region, corresponding to the circulations around the halogen-atom ring, begins at the end point of the first region and extends 15 Bohr beyond the ring center. The bond current strengths calculated using this approach are summarized in Table 2 and Table S1, alongside the corresponding EDDB values. Generally, it is observed that as the size of the bromine- and iodine-atom rings increases in the dications, the current strengths along these rings become more pronounced. Additionally, the current strengths in iodine derivatives are consistently greater than those in the corresponding bromine derivatives. The bond current strengths along the halogen atom rings in the studied doubly oxidized halogenated cycloalkanes are comparable to the σ-current strength of the I_6 ring in $C_6I_6^{2+}$, which, calculated at the same level of theory, was found to be 18.7 nA T^{-1}.[31]

Table 2 Calculated bond current strengths (I, in nA T^{-1}) and EDDB (in a.u.) values for the halogen atom rings in the studied halogenated cycloalkanes in their neutral and dicationic forms. The numbers in parentheses represent the total number of σ-electrons

	I		EDDB	
	Neutral	Dicationic	Neutral	Dicationic
$C_4H_4Br_4$	0.8	2.1	0.376 (8)	4.431 (6)
$C_5H_5Br_5$	1.5	10.1	0.503 (10)	5.114 (8)
$C_6H_6Br_6$	0.8	10.5	0.578 (12)	5.600 (10)
$C_7H_7Br_7$	1.6	17.1	0.747 (14)	6.027 (12)
$C_4H_4I_4$	1.1	4.9	0.377 (8)	4.430 (6)
$C_5H_5I_5$	0.6	14.3	0.465 (10)	5.156 (8)
$C_6H_6I_6$	0.6	15.5	0.511 (12)	5.716 (10)
$C_7H_7I_7$	1.7	23.0	0.676 (14)	6.093 (12)

The EDDB values reveal a significant increase in electron delocalization within the halogen atom rings of all studied molecules upon oxidation. Moreover, this index confirms the absence of cyclic delocalization within the halogen atom units in all the parent non-oxidized molecules. Consistent with the bond current strengths, the EDDB values steadily increase with the ring size and are very similar for iodine- and bromine-atom rings. Notably, the EDDB value of the I_6 ring in $C_6H_6I_6^{2+}$ is even larger than that of the I_6 ring in $C_6I_6^{2+}$.[31] It is important to note, however, that although the EDDB values increase with the ring size, this trend does not directly correlate with the number of σ-electrons on the halogen atoms. For instance, $C_5H_5I_5^{2+}$ and $C_6H_6I_6^{2+}$ contain 8 and 10 σ-electrons distributed among iodine atoms, respectively; yet, the EDDB value of the I_6 ring in $C_6H_6I_6^{2+}$ exceeds that of the I_5 ring in $C_5H_5I_5^{2+}$ by only about 0.5 electrons. Fig. 8 displays EDDB surfaces that further corroborate the σ-aromaticity of bromine- and iodine-atom rings in the dicationic species, while there is no evidence of such σ-aromaticity in the neutral species (Fig. S16).

The bond current strengths along the carbon rings are not significantly affected by oxidation (Table S1). These values indicate relatively weak net circulations along the C–C bond in the molecules examined. Notably, only the cyclobutane ring exhibits somewhat stronger net paratropic circulations, consistent with previous studies.[58,59] The EDDB values (Table S1) support the current density analysis regarding the aromaticity of the carbon rings. The EDDB results do not predict any significant change in the aromatic character of the carbon cycles upon oxidation.

Finally, we investigated the energetic aspect of oxidation induced σ-electron aromaticity using a series of homodesmotic reactions presented in Fig. 9. These reactions were designed to balance changes in charges between neutral and oxidized species, and to equally account for planarity distortions in both reactants and

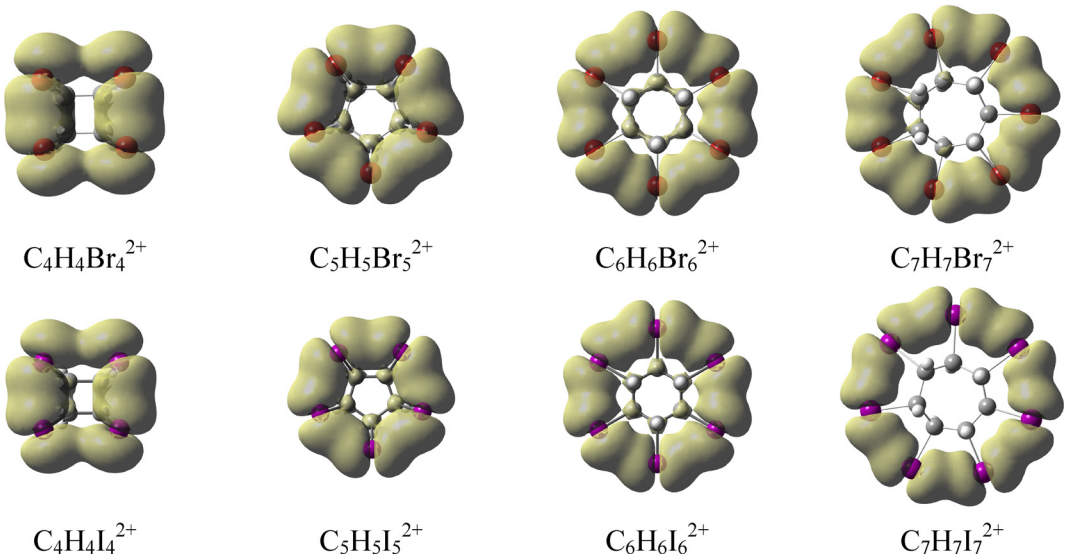

Fig. 8 Top view of the σ-EDDB$_H$ function isosurfaces (isovalue: 0.001 a.u.) for dicationic halogenated cycloalkanes.

products. The homodesmotic reactions were used to calculate the aromatic stabilization energies (ASE).[2,39] As shown in Fig. 9, all dicationic compounds with five-, six- and seven-membered halogen atom rings exhibit stabilization attributed to σ-electron aromaticity. This stabilization appears to vary monotonically with the ring size, except for $C_7H_7I_7^{2+}$. The relatively small ASE value observed for $C_7H_7I_7^{2+}$ may result from incomplete cancellation of planarity deviations between the reactants and products, which is not always straightforward to achieve. In addition, the smallest stabilization from σ-electron delocalization is observed for $C_4H_4I_4^{2+}$, while in $C_4H_4Br_4^{2+}$, this effect is slightly destabilizing. These findings align with the current density distributions for the four-membered rings in these dications, which reveal pronounced localized circulations (Fig. 6 and 7). According to magnetic, electronic and energetic criteria, the dicationic $C_4H_4X_4^{2+}$ species (X = Br and I), although exhibiting more pronounced σ-electron delocalization relative to their neutral analogues, still need to be classified as σ-nonaromatic. These findings can be rationalized by the geometry of the four-membered systems (Fig. 2 and Fig. S3), which, in their dicationic forms, feature two relatively long distances between adjacent halogen atoms. This leads to reduced overlaps between the in-plane lone pairs on the corresponding halogen atoms, thereby preserving stronger σ-electron delocalization along the halogen-atom ring.

The series of molecules studied provides insight into how both the size of the halogen atom ring and the number of σ-electrons involved in cyclic conjugation influence σ-aromatic properties. As demonstrated above, the dications containing four-, five-, six-, and seven-membered halogen atom rings exhibit 6, 8, 10 and 12 σ-electrons, respectively, engaged in cyclic delocalization. The dications $C_nH_nX_n^{2+}$ (n = 5, 6, and 7, and X = Br and I) exhibit σ-aromaticity, suggesting that the observed aromatic behavior does not consistently align with Hückel's $4n + 2$ rule.[34] In particular, this rule appears to hold for rings composed of an even number of halogen atoms, but fails when the ring contains an odd number of halogen atoms.

The obtained results can be interpreted through the CTOCD-DZ approach, which offers valuable insights into the relationship between the electronic structure and molecular magnetic aromaticity.[40,41] A key aspect of this interpretation lies in the selection rules governing virtual excitations: when the product of the symmetries of the occupied and unoccupied orbitals involved in a frontier transition matches the symmetry of an in-plane translation (in-plane rotation), the transition contributes to diatropic (paratropic) current density. In the case of annulenes possessing a C_n symmetry axis, each π-orbital can be characterized by an integer known as the quasi-angular momentum m, which corresponds to half of azimuthal nodes of the orbital. It follows that rotationally and translationally allowed transitions are associated with changes in m of $\Delta m = 0$ and $\Delta m = \pm 1$, respectively. Applying these simple selection rules to the frontier π-orbitals of annulenes allows one to predict the direction of the induced ring currents: $4n + 2$ annulenes sustain diatropic currents, while $4n$ annulenes exhibit paratropic currents. This approach provides a fundamental explanation for the origin of Hückel's aromaticity rule.[60]

To illustrate the differences between halogenated cycloalkanes containing an odd *versus* even number of halogen atoms along their perimeter, Fig. 10 presents molecular orbitals arising from the overlap of tangential p-atomic orbitals on the halogen atoms. For simplicity, a fully symmetric model assuming $D_{n\mathrm{h}}$ symmetry was employed, which omits the explicit presence of hydrogen atoms. This idealized model can be readily applied to the halogen atom rings in the studied molecules, as well as to halogen atom rings in known doubly aromatic species, as the periodo-benzene dication. Accordingly, the orbitals depicted in Fig. 10a and b represent the σ-type MOs of $C_5H_5Br_5^{2+}/C_5H_5I_5^{2+}$ and $C_6H_6Br_6^{2+}/C_6H_6I_6^{2+}$, respectively.

Fig. 10 shows that, in halogen atom rings with $D_{5\mathrm{h}}$ and $D_{6\mathrm{h}}$ symmetries, the set of tangential p-orbitals on the halogen atoms spans the following irreducible representations:

$$\Gamma^{D_{5\mathrm{h}}}_{p_{\mathrm{tangential}}} = \mathrm{E}_2' + \mathrm{E}_1' + \mathrm{A}_2'$$

$$\Gamma^{D_{6\mathrm{h}}}_{p_{\mathrm{tangential}}} = \mathrm{B}_{2\mathrm{u}} + \mathrm{E}_{2\mathrm{g}} + \mathrm{E}_{1\mathrm{u}} + \mathrm{A}_{2\mathrm{g}}$$

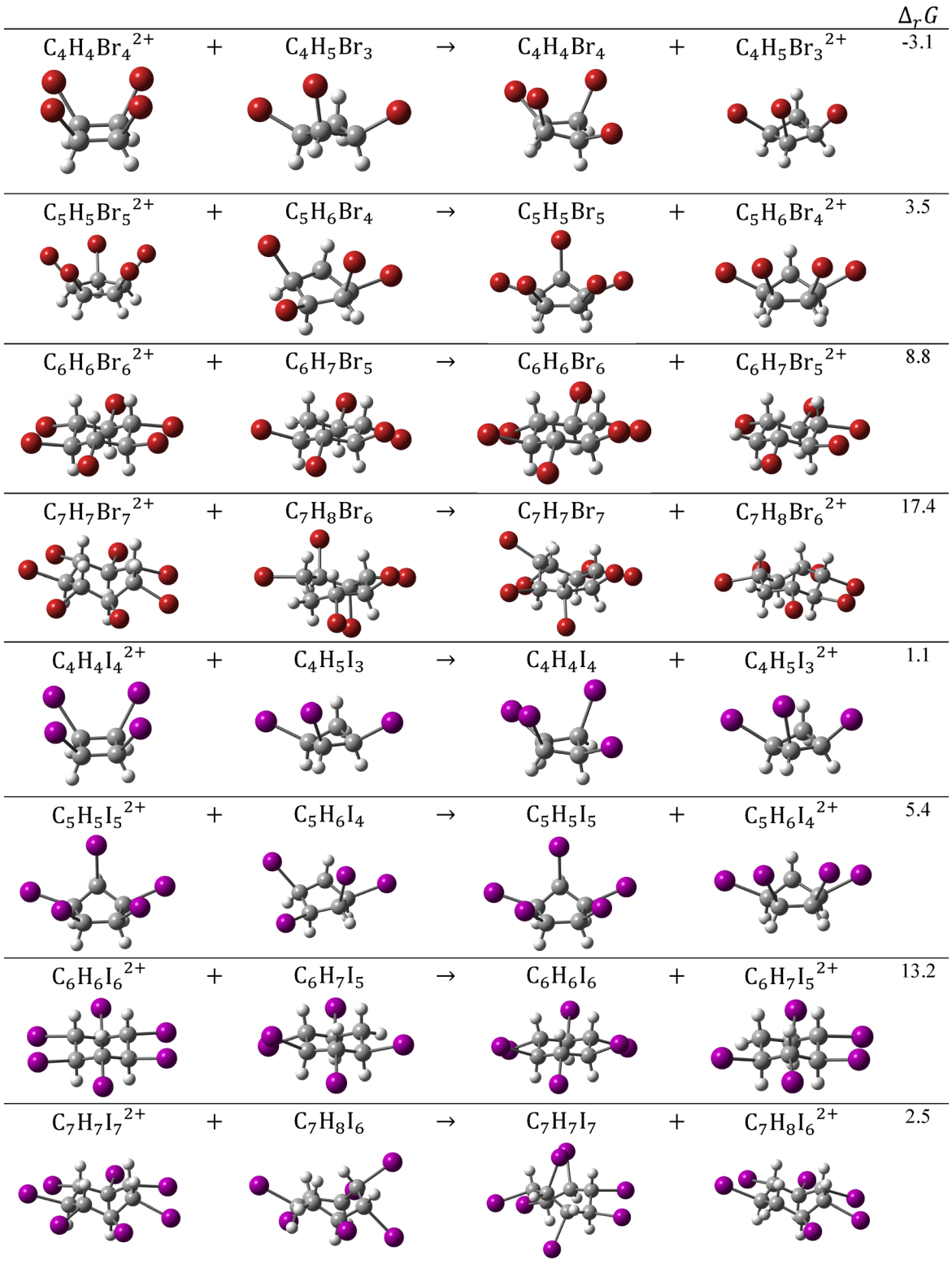

Fig. 9 Homodesmotic reactions employed to evaluate the energetic effect of σ-electron aromaticity in the studied molecules. Optimized structures of all species are shown. The corresponding Gibbs reaction energies ($\Delta_r G$, kcal mol^{-1}) were computed at the B3LYP/def2-TZVP level of theory.

Notably, the quasi-angular momentum quantum number m, defined as half of azimuthal nodal planes, is an integer when the number of halogen atoms is even and a half-integer when the number is odd. By counting nodal planes, one can straightforwardly determine the relative energy ordering of the resulting MOs. The predicted energy levels and orbital shapes from

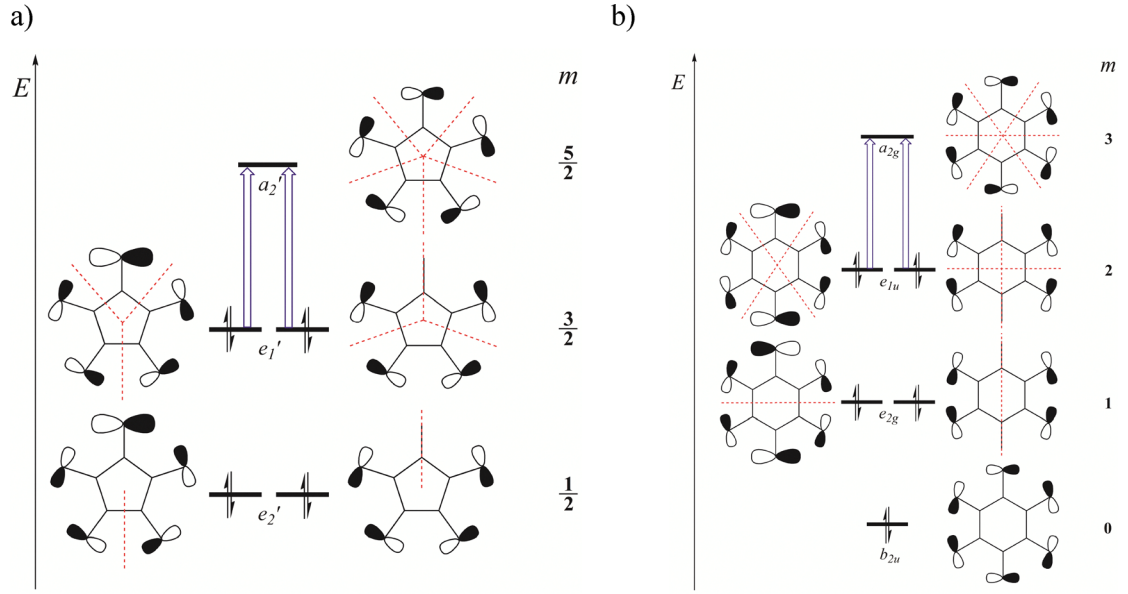

Fig. 10 Idealized representation of σ-type molecular orbitals arising from the overlap of tangential p orbitals on halogen atoms in prototype systems with D_{5h} (a) and D_{6h} (b) symmetries. The quasi-angular moment quantum number m (corresponding to half of the number of azimuthal nodes – indicated by red dotted lines) is given for each orbital. Translationally allowed HOMO–LUMO transitions are shown with straight arrows.

the simple symmetry-based model are in excellent agreement with those obtained from DFT calculations (Fig. 4 and Fig. S10). When the system oxidizes by removing two electrons from the HOMO (a_2' and a_{2g} levels in Fig. 10a and b, respectively), the magnetic response of the resulting dications is governed by virtual transitions from the doubly degenerate occupied orbitals (e_1' and e_{1u} in Fig. 10a and b) to the non-degenerate LUMO. These transitions are transitionally allowed ($\Delta m = 1$) and contribute solely to diatropic current densities. This analysis can be generalized to halogen rings of arbitrary size. For odd-membered rings (*e.g.*, n = 3, 5, 7,...), the $2n - 2\sigma$ electrons fill $(n-1)/2$ doubly degenerate molecular orbitals, all below a single non-degenerate LUMO level (Fig. 11a). For even-membered rings, the σ system consists of two non-degenerate orbitals and $(n/2) - 1$ degenerate pairs in between (Fig. 11a). In both cases, the molecular magnetic response is dominated by virtual excitations involving just four electrons from the highest doubly degenerate level. The proposed energy-level scheme for even-membered rings resembles the structure of Frost–Musulin diagrams traditionally used to describe π-orbitals in aromatic annulenes.[61] In contrast, odd-membered halogen rings follow a "reversed" Frost–Musulin diagram used for annulenes with odd ring size (Fig. 11b).

It is worth noting that, according to the proposed scheme in Fig. 11a, one would expect a diatropic current density induced

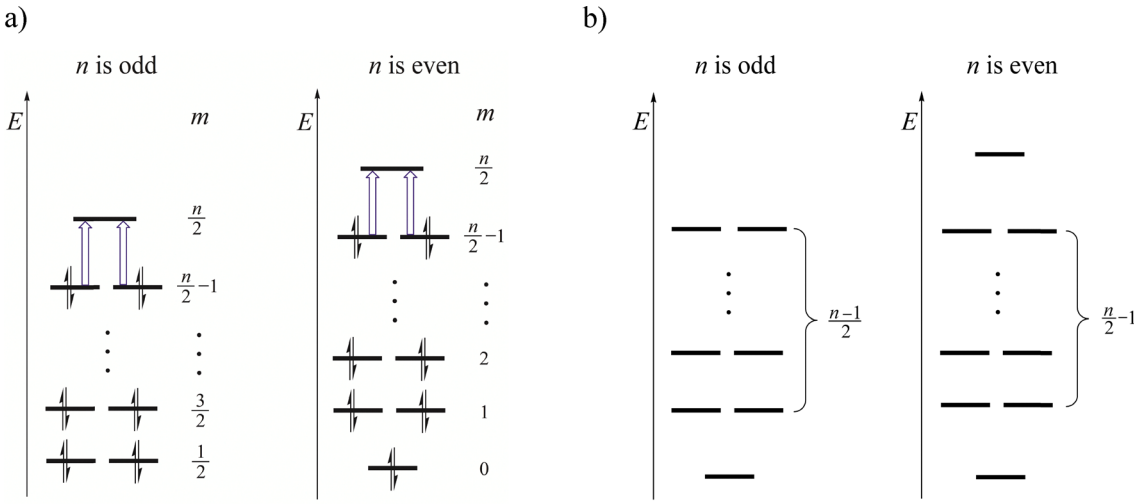

Fig. 11 (a) σ-Type molecular orbital energies of $C_nH_nX_n^{2+}$ arranged based on the values of the quantum number m (corresponding to half of the number of azimuthal nodes). Translationally allowed HOMO–LUMO transitions are shown with straight arrows. (b) Frost–Musulin diagrams for conventional π-molecular orbitals in annulenes C_nH_n.

along the four-membered rings formed by halogen atoms in the dicationic $C_4H_4X_4^{2+}$ species (X = Br, I). As discussed above, this was not observed (Fig. 6 and 7). The limitation of the model can be attributed to the geometry of the four-membered halogen atom rings in these molecules, which deviate significantly from the highly symmetric structure assumed in the model.

Conclusions

In this study, the aromatic character of a series of dicationic halogenated cycloalkanes, in which halogen substituents form cyclic structures, was investigated using magnetic (MICD), electronic (EDDB) and energetic (ASE) indicators. Upon oxidation of the neutral species, we observed a significant shortening of the I–I and Br–Br distances, accompanied by a strong tendency of the halogen rings to adopt planar or nearly planar conformations in their dicationic forms. These structural changes enhance the overlap of in-plane lone-pair orbitals on bromine and iodine, causing the highest-energy σ-type MO to become the LUMO in the dications. Analysis of the σ-delocalized canonical MOs revealed that, for each dication $C_nH_nX_n^{2+}$ (n = 4, 5, 6, and 7, and X = Br and I), the number of cyclically delocalized σ-electrons follows the general formula $2n - 2$.

The MICD results show a clear distinction between the current density distribution of the neutral and oxidized forms. While the neutral species exhibit only localized circulations around individual halogen atoms, the dications display strong global diatropic currents along the perimeter formed by the halogen atoms. An exception is observed for the four-membered ring systems $C_4H_4X_4^{2+}$ (X = Br and I), where σ-electron currents show a slightly localized pattern, rendering these systems σ-nonaromatic. These conclusions are further supported by the EDDB and ASE values.

Notably, the σ-aromaticity found in the studied dications does not always conform to Hückel's rule. Specifically, this rule appears to hold for rings containing an even number of halogen atoms, but breaks down when the ring contains an odd number of halogen atoms. The CTOCD-DZ approach allows prediction and rationalization of magnetic aromaticity in halogen rings of arbitrary size. For both odd- and even-membered rings, the magnetic response is primarily determined by virtual excitations involving just four electrons from the highest occupied, doubly degenerate σ-orbitals to the non-degenerate σ-LUMO.

We believe that our computational findings, supported by a strong theoretical foundation, offer a compelling basis for future investigations and may inspire experimental verification of the predicted σ-aromatic character in dicationic halogenated cycloalkanes.

Author contributions

The manuscript was written through contributions of all authors. All authors have given approval to the final version of the manuscript.

Conflicts of interest

There are no conflicts to declare.

Data availability

The data supporting this article have been included as part of the supplementary information (SI). Supplementary information (SI) is available. See DOI: https://doi.org/10.1039/d5cp03126e.

Acknowledgements

We thank the Serbian Ministry of Science, Technological Development, and Innovation (Agreement No. 451-03-137/2025-03/200122).

References

1 Z. Chen, C. S. Wannere, C. Corminboeuf, R. Puchta and P. von R. Schleyer, *Chem. Rev.*, 2005, **105**, 3842–3888.
2 M. K. Cyrański, *Chem. Rev.*, 2005, **105**, 3773–3811.
3 F. Feixas, E. Matito, J. Poater and M. Solà, *Chem. Soc. Rev.*, 2015, **44**, 6434–6451.
4 R. Gershoni-Poranne and A. Stanger, *Chem. Soc. Rev.*, 2015, **44**, 6597–6615.
5 M. Rosenberg, C. Dahlstrand, K. Kilså and H. Ottosson, *Chem. Rev.*, 2014, **114**, 5379–5425.
6 J. Yan, T. Slanina, J. Bergman and H. Ottosson, *Chem. – Eur. J.*, 2023, **29**, e202203748.
7 M. J. S. Dewar, *Bull. Soc. Chim. Belg.*, 1979, **88**, 957–967.
8 D. Cremer, *Tetrahedron*, 1988, **44**, 7427–7454.
9 A. I. Boldyrev and L.-S. Wang, *Chem. Rev.*, 2005, **105**, 3716–3757.
10 F. Feixas, E. Matito, J. Poater and M. Solà, *Wiley Interdiscip. Rev.: Comput. Mol. Sci.*, 2013, **3**, 105–122.
11 Z. Badri, S. Pathak, H. Fliegl, P. Rashidi-Ranjbar, R. Bast, R. Marek, C. Foroutan-Nejad and K. Ruud, *J. Chem. Theory Comput.*, 2013, **9**, 4789–4796.
12 J. Chandrasekhar, E. D. Jemmis and P. von R. Schleyer, *Tetrahedron Lett.*, 1979, **20**, 3707–3710.
13 E. D. Nelson and H. I. Kenttämaa, *J. Am. Soc. Mass Spectrom.*, 2001, **12**, 258–267.
14 D. J. Sagl and J. C. Martin, *J. Am. Chem. Soc.*, 1988, **110**, 5827–5833.
15 I. Ciofini, P. P. Lainé and C. Adamo, *Chem. Phys. Lett.*, 2007, **435**, 171–175.
16 R. W. A. Havenith, P. W. Fowler, S. Fias and P. Bultinck, *Tetrahedron Lett.*, 2008, **49**, 1421–1424.
17 M. Rauhalahti, S. Taubert, D. Sundholm and V. Liégeois, *Phys. Chem. Chem. Phys.*, 2017, **19**, 7124–7131.
18 S. Furukawa, M. Fujita, Y. Kanatomi, M. Minoura, M. Hatanaka, K. Morokuma, K. Ishimura and M. Saito, *Commun. Chem.*, 2018, **1**, 60.
19 R. Pino-Rios, A. Vásquez-Espinal, O. Yañez and W. Tiznado, *RSC Adv.*, 2020, **10**, 29705–29711.
20 P. W. Fowler and R. W. A. Havenith, *J. Phys. Chem. A*, 2021, **125**, 6374–6383.

21 S. Escayola, N. Proos Vedin, A. Poater, H. Ottosson and M. Solà, *J. Phys. Org. Chem.*, 2023, **36**, e4447.
22 S. Jain, D. Danovich, S. Radenković and S. Shaik, *J. Am. Chem. Soc.*, 2025, **147**, 1092–1100.
23 C. Dari, L. Leyva-Parra, Y. Yang, W. Tiznado and Z. Cui, *Inorg. Chem.*, 2025, **64**, 12429–12434.
24 H. T. Pham, K. Z. Lim, R. W. A. Havenith and M. T. Nguyen, *Phys. Chem. Chem. Phys.*, 2016, **18**, 11919–11931.
25 S. Đorđević and S. Radenković, *Phys. Chem. Chem. Phys.*, 2022, **24**, 5833–5841.
26 J. Barroso, S. Pan and G. Merino, *Chem. Soc. Rev.*, 2022, **51**, 1098–1123.
27 P. W. Fowler, N. Mizoguchi, D. E. Bean and R. W. A. Havenith, *Chem. – Eur. J.*, 2009, **15**, 6964–6972.
28 A. J. Stasyuk, O. A. Stasyuk, M. Solà and A. A. Voityuk, *Chem. Commun.*, 2020, **56**, 352–355.
29 G. V. Baryshnikov, R. R. Valiev, R. T. Nasibullin, D. Sundholm, T. Kurten and H. Ågren, *J. Phys. Chem. A*, 2020, **124**, 10849–10855.
30 I. Rončević, F. J. Leslie, M. Rossmannek, I. Tavernelli, L. Gross and H. L. Anderson, *J. Am. Chem. Soc.*, 2023, **145**, 26962–26972.
31 S. Đorđević, J. Poater, M. Solà and S. Radenković, *Chem. Sci.*, 2025, **16**, 9920–9933.
32 W. Wu, B. Ma, J. I-Chia Wu, P. von R. Schleyer and Y. Mo, *Chem. – Eur. J.*, 2009, **15**, 9730–9736.
33 S. Pelloni, P. Lazzeretti and R. Zanasi, *J. Phys. Chem. A*, 2007, **111**, 8163–8169.
34 M. Solà, *Nat. Chem.*, 2022, **14**, 585–590.
35 P. Lazzeretti, *Phys. Chem. Chem. Phys.*, 2004, **6**, 217–223.
36 D. Sundholm, M. Dimitrova and R. J. F. Berger, *Chem. Commun.*, 2021, **57**, 12362–12378.
37 D. W. Szczepanik, *Comput. Theor. Chem.*, 2016, **1080**, 33–37.
38 D. W. Szczepanik, M. Andrzejak, J. Dominikowska, B. Pawełek, T. M. Krygowski, H. Szatylowicz and M. Solà, *Phys. Chem. Chem. Phys.*, 2017, **19**, 28970–28981.
39 S. W. Slayden and J. F. Liebman, *Chem. Rev.*, 2001, **101**, 1541–1566.
40 E. Steiner and P. W. Fowler, *J. Phys. Chem. A*, 2001, **105**, 9553–9562.
41 E. Steiner and P. W. Fowler, *Chem. Commun.*, 2001, 2220–2221.
42 A. D. Becke, *J. Chem. Phys.*, 1993, **98**, 5648–5652.
43 C. Lee, W. Yang and R. G. Parr, *Phys. Rev. B: Condens. Matter Mater. Phys.*, 1988, **37**, 785–789.
44 S. H. Vosko, L. Wilk and M. Nusair, *Can. J. Phys.*, 1980, **58**, 1200–1211.
45 F. Weigend and R. Ahlrichs, *Phys. Chem. Chem. Phys.*, 2005, **7**, 3297–3305.
46 M. J. Frisch, G. W. Trucks, H. B. Schlegel, G. E. Scuseria, M. A. Robb, J. R. Cheeseman, G. Scalmani, V. Barone, B. Mennucci, G. A. Petersson, H. Nakatsuji, M. Caricato, X. Li, H. P. Hratchian, A. F. Izmaylov, J. Bloino, G. Zheng, J. L. Sonnenberg, M. Hada, M. Ehara, K. Toyota, R. Fukuda, J. Hasegawa, M. Ishida, T. Nakajima, Y. Honda, O. Kitao, H. Nakai, T. Vreven, J. A. Montgomery, J. E. Peralta, F. Ogliaro, M. Bearpark, J. J. Heyd, E. Brothers, K. N. Kudin, V. N. Staroverov, R. Kobayashi, J. Normand, K. Raghavachari, A. Rendell, J. C. Burant, S. S. Iyengar, J. Tomasi, M. Cossi, N. Rega, J. M. Millam, M. Klene, J. E. Knox, J. B. Cross, V. Bakken, C. Adamo, J. Jaramillo, R. Gomperts, R. E. Stratmann, O. Yazyev, A. J. Austin, R. Cammi, C. Pomelli, J. W. Ochterski, R. L. Martin, K. Morokuma, V. G. Zakrzewski, G. A. Voth, P. Salvador, J. J. Dannenberg, S. Dapprich, A. D. Daniels, O. Farkas, J. B. Foresman, J. V. Ortiz, J. Cioslowski and D. J. Fox, *Gaussian 09, Revision B.01*, Gaussian Inc., Wallingford CT, 2009.
47 T. A. Keith and R. F. W. Bader, *Chem. Phys. Lett.*, 1993, **210**, 223–231.
48 T. A. Keith and R. F. W. Bader, *J. Chem. Phys.*, 1993, **99**, 3669–3682.
49 P. Lazzeretti, M. Malagoli and R. Zanasi, *Chem. Phys. Lett.*, 1994, **220**, 299–304.
50 U. Ayachit, *The ParaView Guide: A Parallel Visualization Application*, Kitware, 2015.
51 J. Jusélius, D. Sundholm and J. Gauss, *J. Chem. Phys.*, 2004, **121**, 3952–3963.
52 K. A. Peterson, D. Figgen, E. Goll, H. Stoll and M. Dolg, *J. Chem. Phys.*, 2003, **119**, 11113–11123.
53 R. Ramírez-Tagle, L. Alvarado-Soto, A. Villavicencio-Wastavino and L. Alvarez-Thon, *Phys. Chem. Chem. Phys.*, 2016, **18**, 25751–25755.
54 J. P. Foster and F. Weinhold, *J. Am. Chem. Soc.*, 1980, **102**, 7211–7218.
55 D. W. Szczepanik, *RunEDDB (version 11-Feb-2024)*, **https://aromaticity.eu**, accessed March 15, 2025.
56 M. Antić, B. Furtula and S. Radenković, *J. Phys. Chem. A*, 2017, **121**, 3616–3626.
57 D. Sundholm, H. Fliegl and R. J. F. Berger, *Wiley Interdiscip. Rev.: Comput. Mol. Sci.*, 2016, **6**, 639–678.
58 H. Fliegl, D. Sundholm, S. Taubert, J. Jusélius and W. Klopper, *J. Phys. Chem. A*, 2009, **113**, 8668–8676.
59 G. Monaco, R. Zanasi, S. Pelloni and P. Lazzeretti, *J. Chem. Theory Comput.*, 2010, **6**, 3343–3351.
60 A. Soncini, P. W. Fowler and L. W. Jenneskens, in *Intermolecular Forces and Clusters I. Structure and Bonding*, ed D. J. Wales, Springer, Berlin, Heidelberg, 2005, pp. 57–79.
61 A. A. Frost and B. Musulin, *J. Chem. Phys.*, 1953, **21**, 572–573.

